

Puzzle-AE: Novelty Detection in Images through Solving Puzzles

Mohammadreza Salehi, Ainaz Eftekhari*, Niousha Sadjadi*, Mohammad Hossein Rohban, Hamid R. Rabiee

Department of Computer Engineering

Sharif University of Technology

Tehran, Iran.

Email: smrsalehi@ce.sharif.edu, aeftekhari@ce.sharif.edu, nsadjadi@ce.sharif.edu, rohban@sharif.edu, rabiee@sharif.edu

*Denotes equal contribution

Abstract—Autoencoder (AE) has proved to be an effective framework for novelty detection. The basic idea is that the AEs are expected to have low reconstruction error on the normal data in contrast to the anomalous ones, once trained only on the normal data. Various flavors of AE have achieved state-of-the-art (SOTA) results on simple and semi real-world anomaly detection tasks. However, they do not typically show promising results on other kinds of real-world datasets, which are exhibiting high intra-class variations, such as CIFAR-10. This stems from the fact that in such datasets, highly variegated features like the color of main objects in the foreground, different backgrounds, different poses, and illuminations, etc. make learning a relevant latent space challenging. That is, AEs are not generally able to learn a latent space that solely captures common features of the normal class, resulting in both high false positive and false negative rates due to modeling features that are irrelevant to the normal class. Recently, self-supervised learning has shown great promise in representation learning on such datasets in an unsupervised manner, through solving auxiliary tasks that need a high-level understanding of the data. To this end, we propose a new AE framework that is trained based on solving puzzles on randomly permuted image patches. This particular auxiliary task makes the AE focus on essential properties of the normal class to sort out the puzzle, while the mentioned irrelevant features are likely to be excluded as they do not help in solving the puzzle. Based on this framework, we achieve competitive or superior results compared to *State of the Art* (SOTA) anomaly detection methods on various toy and real-world datasets. Unlike many competitors in this field, the proposed framework is stable, has real-time performance, more general and agnostic to choices of the model hyper-parameters, can work effectively under small sample size settings, and does not require unprincipled early stopping.

1. Introduction

Anomaly/novelty detection (AD/ND) is defined as any digression from the essential features of any given phenomenon. The task of novelty detection is responsible for inferring such kind of features just from training samples of the normal class. For instance, one may have access to MRI brain images of only the healthy subjects and want to distinguish them from the diseased subjects automatically. By inferring *comprehensive* features that are *unique* to the normal samples, one could discern between normal and anomalous datum. Novelty detection methods could be employed to solve such problems by learning features that are specific to the normal class. Then for each test input, one can assess any discrepancy of the extracted features

from that of the normal ones by using specific metrics [1], [2], and [3].

Aside from high *Area Under the Curve* (AUC) of the *Receiver Operating Characteristic* (ROC) curve, a set of desirable traits can be defined in many real-world applications that each ND framework should possess. For instance, high AUC-ROC is not sufficient to guarantee high performance at the test time as one is usually performing on a specific operating point of the reported ROC curve, while AUC involves an average performance across multiple operating points. For most ND applications, points with *True Positive Rate* (TPR) equal or greater than 0.99 are considered to have a more practical use. One would expect the method to have low *False Positive Rate* (FPR) (Positive shows anomaly) in these points. In some other applications like ND in medical images, there are typically a limited number of normal samples available for training. In this case, data efficient frameworks are more desirable. Having a low amount of testing time is sometimes really critical, because most ND applications require real-time recognition of anomalies, e.g. in videos [1], [4]. Another important criterion is the adaptability of a given framework to other datasets. For example, we generally require the model to be agnostic to choices of various hyperparameters, and also have access to well-known criteria to determine when to stop training of the model. In this paper, we compare our method against SOTA along these directions.

Several methods in the literature approach ND by using generative models or one-class classification [5], [6], [7]. GAN [8] is one of the important generative models that is famous for its ability to generate datum that are indistinguishable from the real ones. The mentioned ability makes this intuition that their latent space is semantically meaningful and can be employed for detecting anomalous samples. However, this framework has several caveats like unstable training process, mode collapse [9], [10], non-reproducibility of the results [11], [12], and data hunger that limits their usage in practical scenarios with small sample sizes. Autoregressive density estimation of the normal class have also shown poor performance on novelty detection tasks, and as it is mentioned in [13], they have serious problems with out-of-distribution and novelty detection tasks.

One-class classification methods, [5] and [6], use feature extractors to map inputs from the original space to another space where the normal and anomalous samples are supposed to be well separated. The feature extractor can be a pre-trained network or be trained end-to-end. Using the pre-trained network is sub-optimal, because feature extractor is trained on a different dataset and consequently, in contrast to the end-to-end procedure, is not optimized for the given dataset. Although the end-to-end training extracts more relevant features, it has the problem of converging to trivial solutions and needs confronting techniques

such as early stopping. However, it is often difficult to find a relevant *unsupervised* early stopping criterion, i.e. the one that relies only on the normal samples.

On the other hand, AE-based methods often have straightforward training processes and yield reproducible results. Therefore, we will focus on this framework in this study. It has been observed that an AE that is trained on just normal samples can reconstruct the normal test inputs while fail to reconstruct anomalous test samples [14]. The rationale is that once the encoder is trained on the normal datum, it learns how to extract features that are unique to the normal class. Additionally, as the decoder is trained on the normal samples, it supposedly learns how to reconstruct them properly. Thus, one would expect the encoder to output meaningful latent features if and only if it is given a normal sample. The decoder would consequently perfectly reconstruct the input from the meaningful features. This suggests that we can use the reconstruction error as a criterion to compute the abnormality score of the test inputs.

It has been shown in *Adversarial Robust Trained Autoencoder* (ARAE) [15] that this premise does not hold necessarily, and the AE also reconstructs the anomalous samples well. As a remedy, the mentioned study forces the AE to learn more semantically meaningful features in its latent space through adversarial perturbations. This reduces both false negative and false positive rates, which is caused by reducing the AE generalization on the anomalous samples. However, all kinds of AEs from ARAE to the simple AE have the issue of low-quality reconstruction on complex datasets such as CIFAR-10 [16]. The reason for this phenomenon should be investigated in the training procedure of AEs, which tries to model pixel intensities by a complex function that is represented by the decoder. Modeling the input image at the pixel level could deprive the AE of a more general abstraction, which means finding fallacious relationships between unnecessary features.

Some recent studies strive to force the AE to learn semantic features beyond pixel-level abstraction. For example, beta *Variational Autoencoder* (VAE) [17] tries to find disentangled latent space that prunes a lot of irrelevant pixel-level relationships. Also, self-supervised learning methods have shown great potential to learn semantically meaningful features. Stunning unsupervised classification accuracy on the ImageNet dataset [18] in [19], [20] and [21] has attracted a lot of attention to this field. Recently [22] has used jigsaw puzzle-solving to solve the feature imbalance problem of image generation in the VAEs. [23] is the first one-class classification method that utilizes self-supervised learning, which achieves great performance on the CIFAR-10 dataset [16]. However, we will show that in addition to the mentioned deficiencies of one-class classification methods, they are not even as good as the simple AE on real-world datasets like MVTecAD [24] and CT brain images^{1 2}. All of this guide us to manipulate adversarial robust training [25], [26], self-supervised learning [27], [28] and U-Net [29] (as the AE structure) to build a new framework solving the novelty detection problems with completely different insight from traditional ones. Our framework shows great performance on large gamut of datasets. To the best of our knowledge, our work is the first study that produces a framework *without any need to design unprincipled early stopping criterion*, while also produces stable and reproducible results. Our main contributions include addressing the following issues:

- 1) **AE normal sample generalization:** Significantly re-

lieving the AE framework normal sample generalization problem on the complex real-world datum. This achieves by learning beyond pixel-level abstraction using self-supervised training, removing some of the shortcuts by adversarial robust training, and improving the quality of generated images by training the whole framework similar to *Generative Adversarial Network* (GAN).

- 2) **Method Stability:** The generative nature of our proposed self-supervised method helps in reaching a stable model across the training epochs. We empirically notice the lack of this property in the earlier self-supervised frameworks for the anomaly detection.
- 3) **Shortcuts in the Jigsaw:** Relieving the shortcut problem of the jigsaw puzzle pretext task that is traditionally solved by manual jittering, automatically by adversarial robust training.
- 4) **Method Evaluation:** Introducing new practical criteria, FPR at a high TPR, and robustness to the test-time adversarial attacks, that have not been tested on any recent SOTA models.
- 5) **Method Generality:** Competitive or better than SOTA performance on a *wide* range of problems without any need to unprincipled early stopping, and with a stable training process, yielding robust and reproducible results.

2. Related Works

As mentioned earlier two major approaches to the novelty detection are AE based and one-class classification methods. We will briefly review these methods next.

Latent space autoregression (LSA) [30] is such an AE based approach, which fits an autoregressive model to the AE bottleneck layer. By jointly training an autoregressive model and AE, it is able to learn compact latent space for the normal samples. Hence not only anomalous samples would have high reconstruction errors, but also the value of their bottleneck layer would have a lower probability than the normal ones. This probability is called “surprise score” in LSA. At testing time, the surprise score is added to the mean reconstruction error, and the sum is then thresholded to determine the class of the given sample.

OCGAN [31] is an AE based approach that uses an AE that is jointly trained with reconstruction and generative adversarial error losses. In contrast to the LSA, it tries to force the encoder output distribution to be approximately uniform. This causes the decoder to reconstruct just normal outputs for both normal and anomalous inputs, which results in a higher mean squared error for abnormal input datum. [4] is the first AE framework that uses memory in a non-parametric approach for ND. When an input is passed to the AE, it is searched within the memory to find embeddings that match that of the input. Then, based on the combination of these embeddings, a new one is made, and is passed through the decoder.

Deep SVDD [5] is a one-class classification method that tries to convert data from original space to some other space by using deep neural networks. During the training process, it tries to put normal datum in a circle with a predefined center in a new space and then iteratively reduces its diameter. Because of the problem of finding trivial solutions, it uses early stopping and puts some constraints on the activation functions of layers. *Geometric Transformations* (GT) [23] is another one-class

1. www.kaggle.com/felipekitamura/head-ct-hemorrhage

2. www.kaggle.com/navoneel/brain-mri-images-for-brain-tumor-detection

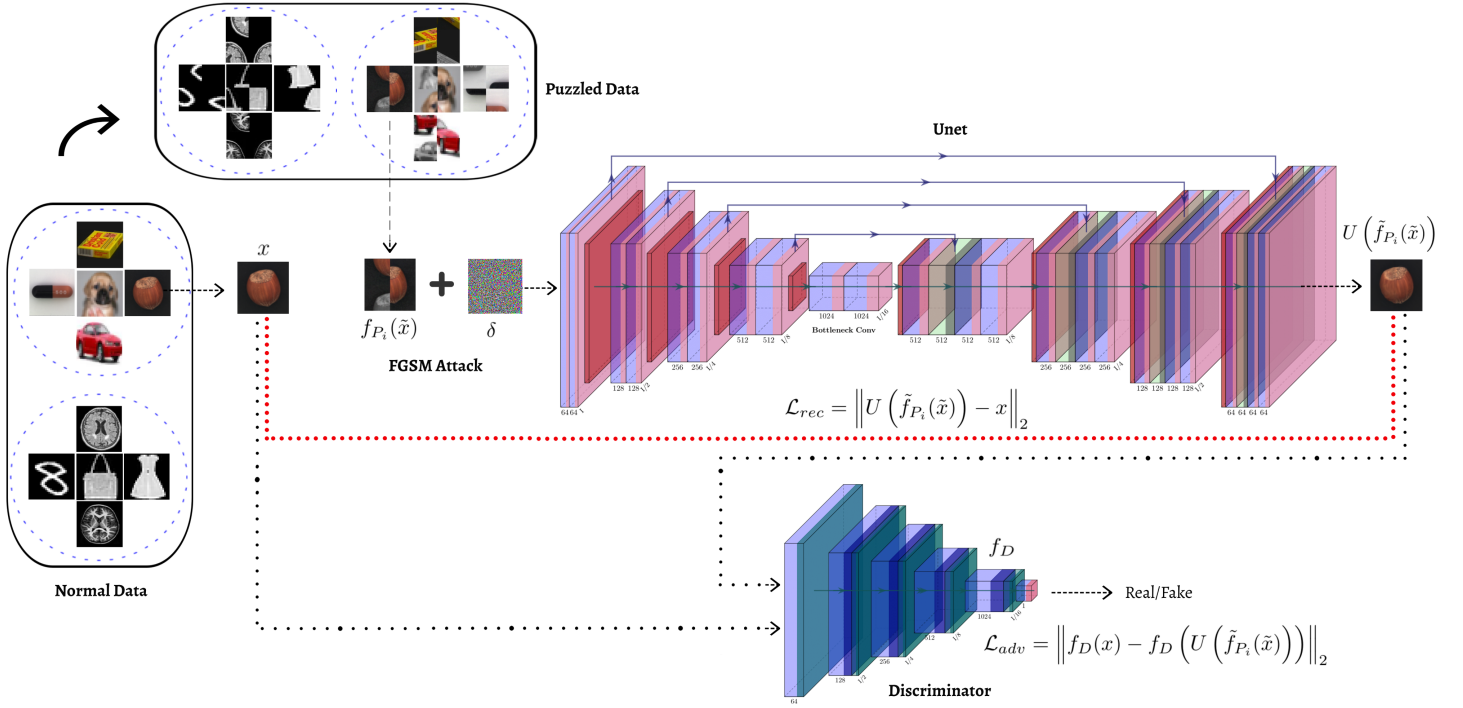


Figure 1: Overview of our proposed Anomaly Detection framework.

classification method that also uses self-supervised learning. It makes a set of different transformations on training data then by using a classifier tries to guess which transformation is done on each input. Premising that in spite of anomalous inputs, normal ones are classified correctly at the testing time.

AnoGAN [32] is the first GAN based framework for novelty detection. It trains a GAN on the normal training datum. Then at the testing time, it looks for an appropriate latent vector such that the mean generator reconstruction error becomes lower than a certain threshold. Because of the high testing time in AnoGAN, [33] introduced an improved version of AnoGAN, which does not need to solve any optimization problem at the testing time (Ganomaly). Ganomaly employs VAE [34] and GAN [8] frameworks to achieve this goal. Therefore, rather than solving the optimization problem at the testing time, it just uses the encoder part of VAE to obtain the desirable latent vector.

3. Method

As mentioned before self-supervised learning methods seem great for extracting semantically meaningful and generalizable features. The main deficiency of AEs is the inability to generalize normal data on complex datasets under a limited number of training normal samples. For example, in the class car of CIFAR-10 dataset, AE may reconstruct a normal red car but gets confused by an exactly similar input with a different color. Making rich datasets with millions of datum may solve this deficiency but it is against the premises of novelty detection. Because in many real applications of novelty detection, it is assumed that there are not any rich datasets for the normal samples that includes every possible variation. Besides, it could also be infeasible to build such a dataset. In order to use potentials of AEs and also reduce its mentioned important weaknesses, we propose the Puzzle-AE framework.

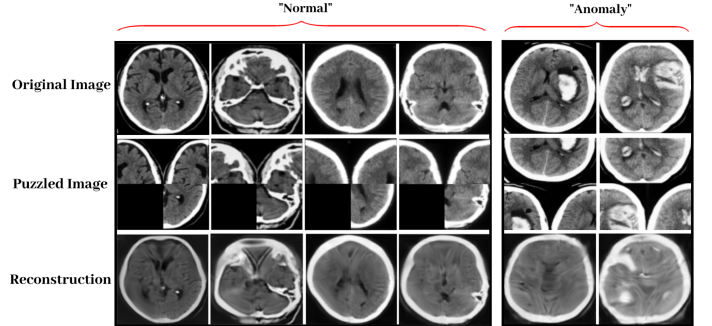


Figure 2: Visualization of the proposed method on Head CT dataset. First row is the original input, second row is the puzzled input mingled by inpainting task, and the third row is the unpuzzled output solved by the model.

3.1. Model Training

The proposed framework is illustrated schematically in the Fig. 1. U-Net [35] architecture is used as our base framework that has a similar structure to AE and is also popular because of its ability to reconstruct high-quality images, which is used by segmentation methods [35], [36], [37]. However, we pass puzzled input rather than noisy or original one and it is expected from U-Net [35] to reconstruct the right order images. Then U-Net [35] is trained by *Mean Square Error* (MSE) loss of its output and original input. Some instance pictures of normal input dataset are shown by Figs. 2, 5 and 6.

Puzzle Making: According to the principles of self-supervised learning, we use puzzle-solving as our pretext task.

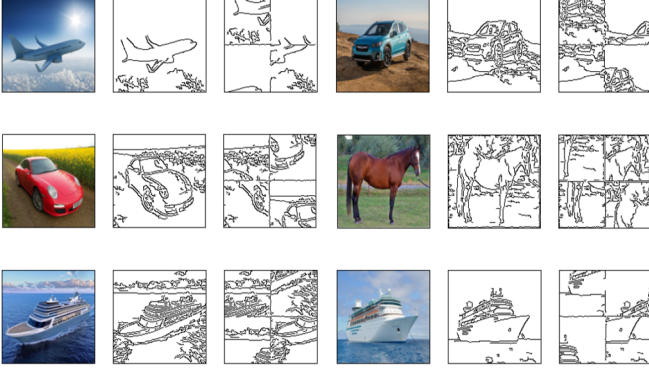


Figure 3: As it is shown, by puzzling an image, some trivial features are produced that conduct the model to learn trivial solutions of doing the puzzle. For example, model could understand the number of displacements just by noticing the vertical and horizontal lines.

During the puzzle making procedure, each input image is split into 4 partitions and then selected a random permutation of these partitions with at least 2 displacements. The 4 partitions puzzle is chosen because it is the most evident way of making puzzle resulted in agnosticism about datasets. In order to obtain better features, puzzle making procedure is combined with inpainting (for gray-scale images) or colorization (for colorful images). Thus a partition is selected randomly and fully blacked at the inpainting cases. Otherwise the color of that partition is converted to black and white (average each pixel value along the channel dimension) at the colorization cases. Suppose we have a given input $x \in \mathcal{X}$, where \mathcal{X} denotes the entire training dataset. We first split this input into 4 partitions and convert a random partition to black or black and white to obtain \tilde{x} . We show the set of puzzles as $\mathcal{F} = \{f_{P_i}(\cdot) \mid i = 1, \dots, K\}$ where K is equal to 23 in case of having 4 partitions in each puzzle and considering all the possible permutations of the partitions with at least 2 displacements. $f_{P_i}(\tilde{x})$ denotes a specific permutation of the 4 partitions in which one partition is fully blacked or converted to black and white.

Puzzle Making for Texture Images: The defined set of puzzles \mathcal{F} determines the ambiguity of our self-supervised learning task. As mentioned in [27], a good self-supervised learning task should not be ambiguous. Now considering texture-like images such as 5 texture categories in MVTEC-AD dataset, all the 4 partitions in the puzzled image are mostly similar. Consequently, finding the right solution for all the 23 permutations of the partitions would be impossible. Therefore, to make our self-supervised learning task less ambiguous, only the 6 different permutations of the partitions with exactly 2 displacements are considered in our puzzle set \mathcal{F} which means K would be equal to 6 in this case.

Adversarial Robust Training: There exist trivial solutions in self-supervised learning methods that are reputed as shortcut solutions in the literature. Here also exist shortcut solutions like: finding low-level statistics of different partitions and using them to do the puzzle, finding partitions border edges in the puzzled input in order to extract the relational position of partitions, etc. In order to relieve these shortcut problems, we use adversarial robust training as in [15] (that can be viewed as automatic shortcut removal) and all of the inputs in both training and testing time are with at least two displacements in their partitions. As PGD [25] is so time consuming, we use FGSM [38] rather than it. Fig. 4 and Fig. 3 show the aforementioned problem and the

effect of adversarial robust training on it. As it is shown, FGSM [38] noises are added to image purposefully to relieve effect of low level statistics like edges, each patch channel-wise mean and etc in puzzle solving procedure.

$$\begin{cases} 1. \delta = \text{Uniform}(-\epsilon, \epsilon) \\ 2. \delta = \delta + \alpha \cdot \text{sign}(\nabla_x \|U(f_{P_i}(\tilde{x}) + \delta) - f_{P_i}(\tilde{x})\|_2) \\ 3. \delta = \max(\min(\delta, \epsilon), -\epsilon) \\ 4. \tilde{f}_{P_i}(\tilde{x}) = f_{P_i}(\tilde{x}) + \delta, \end{cases} \quad (1)$$

Eq. 1 shows more details about manipulation of FGSM [38] in the proposed framework. $U(\cdot)$ indicates the U-Net network, ϵ is the attack magnitude, and α is the step size. $\tilde{f}_{P_i}(\tilde{x})$ is the adversarial sample obtained from the puzzled input $f_{P_i}(\tilde{x})$.



Figure 4: Effect of FGSM [38] on depletion of trivial solutions. As the Figure shows, FGSM [38] tries to make specific anti-shortcut noises that appear similar to number 8. This forces the network not to overfit on low level statistics automatically. Heat map shows the normal image with better noise clarification.

Adversarial Training and Total Loss: The whole mentioned framework is also trained similar to GAN framework [8] to improve the quality of the produced images. Better quality is obtained because of the ability of the adversarial training to converge to one mode in spite of MSE that converges to average of different modes [39], [2], [40]. We define the reconstruction loss \mathcal{L}_{rec} as the \mathcal{L}_2 distance between the original input x which is drawn from the input data distribution p_x , and the solved puzzle at the output of the U-Net network $U(f_{P_i}(\tilde{x}))$:

$$\mathcal{L}_{rec} = \mathbb{E}_{x \sim p_x} \|U(f_{P_i}(\tilde{x})) - x\|_2. \quad (2)$$

Similar to [33], feature matching loss in the adversarial training is used. $f_D(\cdot)$ denotes a function representing an intermediate layer of our discriminator D . The adversarial loss \mathcal{L}_{adv} is defined as follows:

$$\mathcal{L}_{adv} = \mathbb{E}_{x \sim p_x} \|f_D(x) - \mathbb{E}_{x \sim p_x} f_D(U(f_{P_i}(\tilde{x})))\|_2. \quad (3)$$

Finally, the total loss used as our total training objective is defined as:

$$\mathcal{L}_{total} = \mathcal{L}_{rec} + \lambda \mathcal{L}_{adv}, \quad (4)$$

where λ is a hyper-parameter defining the weight of the \mathcal{L}_{adv} term in the total loss.

3.2. Model Testing

The same puzzle-making procedure is used for evaluation. We split each test data into 4 partitions and consider all the K permutations of these partitions with at least 2 displacements

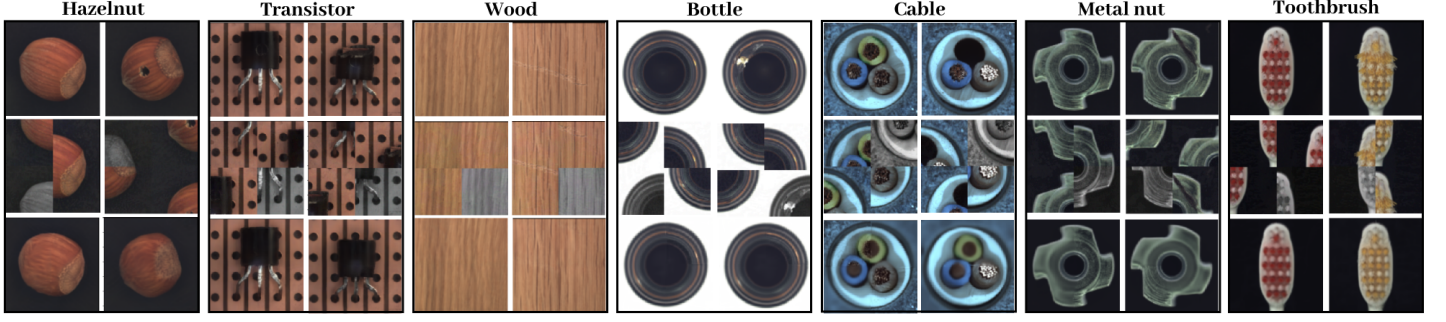


Figure 5: Visualization of the proposed method on MVTEC-AD [24] dataset. First row is the original image, second row is the puzzled input mingled by colorization and third row is the model’s output. For each category, first column is a normal input and the second column is an anomalous one.

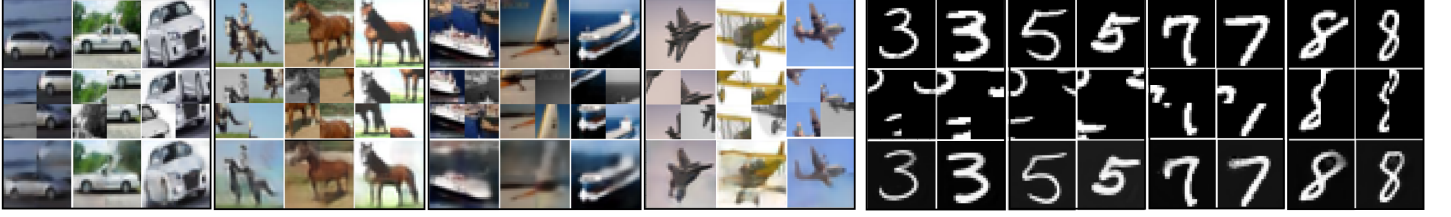


Figure 6: Visualization of the proposed method on CIFAR-10 [16] and MNIST [41] datasets. First row is the original input, second row is the puzzled input mingled by one of the colorization or inpainting tasks and the third row is the unpuzzled output.

without any inpainting or colorization auxiliary task. Suppose x is a given test data and the i^{th} permutation is used for the puzzle-making process to obtain $f_{P_i}(x)$. The anomaly score for this specific permutation is defined as:

$$\mathcal{S}_{test}^i = \|U(f_{P_i}(x)) - x\|_2. \quad (5)$$

Error Normalization: Since solving each of the K puzzles have different difficulties for the model, the reconstruction error for some puzzles can be much larger than the others. Hence, different reconstruction errors can be obtained for a single input depending on the permutation used for the puzzle-making process. Therefore, we use validation data to normalize these errors over all the permutations. For this purpose, the average reconstruction error over all the validation data is computed for every single permutation. During test time, each reconstruction error is divided by the average error of validation data corresponding to that permutation :

$$\mathcal{S}_{test}^{'i}(x) = \frac{\|U(f_{P_i}(x)) - x\|_2}{\mathbb{E}_{x \sim p_x} \|U(f_{P_i}(x)) - x\|_2}. \quad (6)$$

Finally, min, max and average anomaly score for all the K permutations of a single test data is computed:

$$\mathcal{S}_{test}(x) = \{\min \text{ OR } \max \text{ OR } avg\}_{1 \leq i \leq K} \{\mathcal{S}_{test}^{'i}(x)\}. \quad (7)$$

The experiments show that taking the max is better for simple datasets, and as the dataset gets more complex, taking the average or min would yield better results. Therefore, to avoid unnecessary confusion and complexity in our performance measurement, we report the results by taking the max for toy datasets and taking the avg for real-world datasets.

Fig. 5 shows the output of the model for two different normal and anomalous inputs of 7 categories of the MVTEC-AD [24]

dataset. Right column of Fig. 7 shows outputs of the model trained on the class car of the CIFAR-10 [16] dataset for some anomalous inputs.

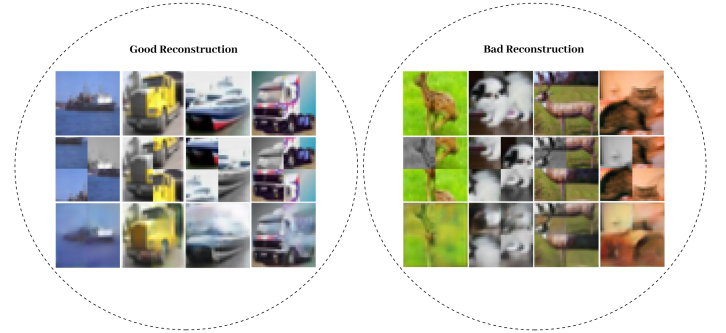


Figure 7: Outputs of the model trained on the class car of the CIFAR-10 [16] dataset for anomalous inputs. As it shows, some samples of the truck class are also unpuzzled well, which could be for high similarity between main features of car and truck. The same implications exist for some of the ship class samples.

4. Experiments

In this section, we validate our method by conducting extensive experiments. We consider multiple commonly used datasets such as MNIST, Fashion-MNIST, CIFAR-10 and COIL-100, and also real-world datasets like MVTEC-AD and medical datasets for evaluating our model. We show that despite the simple approach, our proposed method outperforms several state-of-the-art approaches on these datasets.³

3. Code to reproduce the results is provided at https://github.com/Niousha12/Puzzle_Anomaly_Detection.

TABLE 1: Area under the ROC curve in % for several datasets. As it is shown, Puzzle AE surpass the SOTA by 7% on average on the CIFAR-10 [16] dataset while it is still competitive on the other ones.

Dataset	Method	0	1	2	3	4	5	6	7	8	9	Mean
MNIST [41]	ARAE [15]	99.8	99.9	96.0	97.2	97.0	97.4	99.5	96.9	92.4	98.5	97.5
	OCSVM [6]	99.5	99.9	92.6	93.6	96.7	95.5	98.7	96.6	90.3	96.2	96.0
	AnoGAN [32]	96.6	99.2	85.0	88.7	89.4	88.3	94.7	93.5	84.9	92.4	91.3
	DSVDD [5]	98.0	99.7	91.7	91.9	94.9	88.5	98.3	94.6	93.9	96.5	94.8
	CapsNet _{pp} [42]	99.8	99.0	98.4	97.6	93.5	97.0	94.2	98.7	93.9	99.0	97.7
	OCGAN [31]	99.8	99.9	94.2	96.3	97.5	98.0	99.1	98.1	93.9	98.1	97.5
	LSA [30]	99.3	99.9	95.9	96.6	95.6	96.4	99.4	98.0	95.3	98.1	97.5
OURS		99.6 ± 0.004	99.93 ± 0.004	97.12 ± 0.083	96.97 ± 0.039	97.70 ± 0.017	98.43 ± 0.022	99.29 ± 0.041	98.26 ± 0.036	94.14 ± 0.073	98.57 ± 0.082	98.00
Fashion-MNIST [43]	ARAE [15]	93.7	99.1	91.1	94.4	92.3	91.4	83.6	98.9	93.9	97.9	93.6
	OCSVM [6]	91.9	99.0	89.4	94.2	90.7	91.8	83.4	98.8	90.3	98.2	92.8
	DAGMM [44]	30.3	31.1	47.5	48.1	49.9	41.3	42.0	37.4	51.8	37.8	41.7
	DSEBM [45]	89.1	56.0	86.1	90.3	88.4	85.9	78.2	98.1	86.5	96.7	85.5
	DSVDD [5]	98.2	90.3	90.7	94.2	89.4	91.8	83.4	98.8	91.9	99.0	92.8
	LSA [30]	91.6	98.3	87.8	92.3	89.7	90.7	84.1	97.7	91.0	98.4	92.2
	OURS(4-parts)	91.37 ± 0.200	98.96 ± 0.019	89.34 ± 0.056	92.04 ± 0.317	91.04 ± 0.087	90.73 ± 0.189	82.39 ± 0.077	98.23 ± 0.026	91.02 ± 0.190	97.52 ± 0.200	92.26
OURS(9-parts) ^a		91.73 ± 0.621	98.74 ± 0.133	89.92 ± 0.252	91.94 ± 0.612	89.69 ± 0.566	93.54 ± 0.606	84.90 ± 0.405	98.78 ± 0.078	92.30 ± 1.178	98.46 ± 0.169	93.00
CIFAR-10 [16]	ARAE [15]	72.2	43.1	69.0	55.0	75.2	54.7	70.1	51.0	72.2	40.0	60.23
	OCSVM [6]	63.0	44.0	64.9	48.7	73.5	50.0	72.5	53.3	64.9	50.8	58.56
	AnoGAN [32]	67.1	54.7	52.9	54.5	65.1	60.3	58.5	62.5	75.8	66.5	61.79
	DSVDD [5]	61.7	65.9	50.8	59.1	60.9	65.7	67.7	67.3	75.9	73.1	64.81
	CapsNet _{pp} [42]	62.2	45.5	67.1	67.5	68.3	63.5	72.7	67.3	71.0	46.6	61.2
	OCGAN [31]	75.7	53.1	64.0	62.0	72.3	62.0	72.3	57.5	82.0	55.4	65.66
	LSA [30]	73.5	58.0	69.0	54.2	76.1	54.6	75.1	53.5	71.7	54.8	64.1
OURS		78.93 ± 0.203	78.05 ± 0.755	69.95 ± 0.344	54.88 ± 0.410	75.46 ± 0.204	66.04 ± 0.430	74.76 ± 0.280	73.30 ± 0.468	83.34 ± 0.256	69.96 ± 0.461	72.47

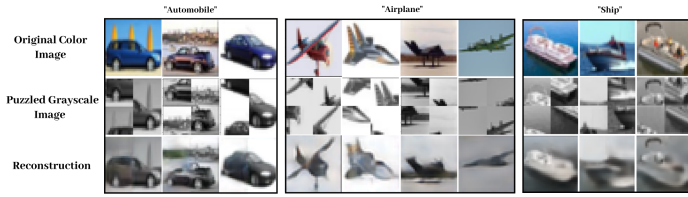


Figure 8: Effect of converting images to gray-scale on the model learned features for some classes like car, plane and ship of the CIFAR-10 [16] dataset. As it is shown, the model can produce perfect outputs even for gray-scale inputs.

4.1. Experimental Setup

Datasets. We consider 7 datasets for evaluating our method: MNIST, Fashion-MNIST, CIFAR-10, COIL-100, MVTecAD, and 2 medical datasets (Head CT (hemorrhage) and Brain MRI Images for Brain Tumor Detection). We introduce each of these datasets as follows:

- **MNIST [41]** consists of 70,000 28×28 gray-scale handwritten digit images from 0 to 9 divided equally between classes. There are 60,000 training images and 10,000 test images.
- **Fashion-MNIST [43]** is a dataset similar to MNIST consisting of 70,000 gray-scale images of 10 fashion product categories with 7000 images per category. There are 60,000 training images and 10,000 test images.
- **CIFAR-10 [16]** is a dataset with 60,000 32×32 color images in 10 classes, with 6000 images per class. It consists of 50,000 training images and 10,000 test images.
- **COIL-100 [46]** is a dataset comprising 7200 128×128 color images of 100 object classes. There are 72 images of each object in different poses.
- **MVTecAD [24]** is an industrial dataset with more than 5000 high-resolution images in fifteen different categories of objects and textures. Each category contains both normal images used for training and anomalous images with various kinds of defects used for testing. We downscale all images in this dataset to the size

128×128 . We also use zoom data augmentation to create 800 training images for each class.

- **Head CT (hemorrhage)** is a medical dataset containing 100 128×128 normal head CT images and 100 with hemorrhage.
- **Brain MRI Images for Brain Tumor Detection** is a medical dataset that consists of 98 256×256 normal MRI images and 155 with brain tumors.

Model Configuration and Hyperparameters. We use the standard U-Net architecture without the batchnorm layers [51] as our base framework which is trained to reconstruct right order images. Also, the standard discriminator introduced in DCGAN [52] is used as our next subnetwork which is trained to classify the original input and output of the U-Net [35] as real or fake. We use Adam optimizer [53] for training both networks. The learning rate is initially set to $1e-3$ for the U-Net [35] and $2e-4$ for the discriminator. We use a learning rate scheduler to multiply the learning rate by 0.8 when the minimum amount of loss doesn't change for 50 subsequent epochs [54]. We use the FGSM attack for adversarial robust training of the model. We train the model until convergence of the loss function with a batch size of 8 for MVTecAD [24] and medical datasets and a batch size of 128 for the rest of the datasets.

Evaluating Protocols. We define the data partitions used for the training-testing procedure. For MNIST, Fashion-MNIST, CIFAR-10, and COIL-100 we select one class as the normal class, and the samples from the other classes are considered anomalous.

We first mention the 2 protocols used for training and testing in the literature of unsupervised novelty detection:

- **Protocol 1:** In this protocol, 80% of normal samples are used for training and the remaining 20% is used at test time. The rest of the test set is made by random sampling from the anomalous classes so that the number of normal and anomalous samples are equal in the test data.
- **Protocol 2:** This protocol uses the original training-testing split of the dataset. Training samples of the

4. The whole procedure is completely the same as the 4-part puzzle. However, the datum is extended to 30×30 and partitioned into 9 parts where 6 parts are permuted and 1 is fully blacked randomly.

TABLE 2: Area under the ROC curve in % on MVTec AD [24] dataset. As it is shown, Puzzle AE surpass other SOTAs significantly and about 4.6% with respect to the best previous SOTA.

Method	Bottle	Hazelnut	Capsule	Metal Nut	Leather	Pill	Wood	Carpet	Tile	Grid	Cable	Transistor	Toothbrush	Screw	Zipper	Mean
AVID [39]	88.0	86.0	85.0	63.0	58.0	86.0	83.0	70.0	66.0	59.0	64.0	58.0	73.0	66.0	84.0	73.0
AE _{SSM} [47]	88.0	54.0	61.0	54.0	46.0	60.0	83.0	67.0	52.0	69.0	61.0	52.0	74.0	51.0	80.0	63.0
AE _{L2} [47]	80.0	88.0	62.0	73.0	44.0	62.0	74.0	50.0	77.0	78.0	56.0	71.0	98.0	69.0	80.0	71.0
AnoGAN [32]	69.0	50.0	58.0	50.0	52.0	62.0	68.0	49.0	51.0	51.0	53.0	67.0	57.0	35.0	59.0	55.0
LSA [30]	86.0	80.0	71.0	67.0	70.0	85.0	75.0	74.0	70.0	54.0	61.0	50.0	89.0	75.0	88.0	73.0
OURS	94.24 ± 0.10	91.21 ± 0.13	66.88 ± 0.23	66.33 ± 0.10	72.86 ± 0.86	71.63 ± 0.11	89.51 ± 0.63	65.73 ± 0.37	65.48 ± 0.12	75.35 ± 0.60	87.90 ± 0.10	85.96 ± 0.12	97.79 ± 0.05	57.81 ± 1.12	75.74 ± 0.13	77.63

TABLE 3: Area under the ROC curve in % on COIL-100 [46] dataset. As it is shown, Puzzle AE reaches one of the SOTAs and surpass the others significantly.

Outlier Pursuit [48]	DPCP [49]	ALOCC DR [7]	ALOCC D [7]	GPND [50]	OCGAN [31]	OURS
90.8	90.0	80.9	68.6	96.8	99.5	99.3

TABLE 4: Area under the ROC curve in % on real-world medical datasets. As it is shown, Puzzle AE has significant improvement with respect to the other AE based SOTA methods.

		LSA* [30]	OCGAN* [31]	OURS
Head CT (hemorrhage)	AUC	81.67 ± 0.358	51.22 ± 3.626	86.43 ± 0.04
	FPR	0.81	1.00	0.70
Brain MRI Images for Brain Tumor Detection	AUC	95.61 ± 1.433	91.74 ± 3.050	96.34 ± 0.031
	FPR	0.40	0.60	0.50

normal class are used for training and validation, and the whole test data of all classes are used for evaluation.

We use protocol 1 for the COIL-100 [46] dataset. We randomly take one class as the normal class and use samples of other classes as anomalous data. We repeat this process 30 times and average the results. For the medical datasets, we randomly select 10 normal images and use them along with the anomalous ones for the test data. The rest of the normal images are used for the training. For MVTecAD [24] dataset, we use the given train and test set for each class. We perform zoom augmentation to create 800 training images for each category. Protocol 2 is used for all other datasets to train and test the model. 15% of the training data is reserved for validation in each dataset.

We evaluate the performance using the AUC of the ROC curve which is commonly used for measuring performance in anomaly detection tasks.

4.2. Testing Time

To compare execution time of our method with GT [23], we run CIFAR-10 experiment on NVIDIA-GTX1080ti processor with 12 Gigabytes RAM and with the same batch size. It has been observed that our testing routine has $4.7\times$ better execution performance.

4.3. Results

In this section, we provide the results of our method on the mentioned datasets, and we compare them with some popular approaches on these datasets. Most of the results are declared with some variance like in Tables. 1, 2, 4, and 8. In each of them, the corresponding model is tested in each of the last 20 epochs of the training process, and the mean and variance of these 20 test results are reported. Most of the results shown for other methods are the reported results in the original papers. We used the officially released source code of LSA [30], GT [23], and OCGAN [31] to produce the rest of the results. We used the reported training setting for each dataset if mentioned in the

paper. Otherwise, we trained the model until convergence and producing the expected results.

AUC comparison with SOTA methods: The AUC results are presented for MNIST [41], Fashion-MNIST [43] and CIFAR-10 [16] in Table. 1, in which Puzzle-AE is compared with recent SOTAs on these datasets. Table. 2 shows comparison between Puzzle-AE and other SOTA methods on real-world, industrial dataset MVTecAD [24]. Table. 3 shows results of Puzzle-AE on COIL-100 [46] dataset. In order to show the effectiveness and generalization of the proposed framework, two extra experiments are conducted on 2 different medical datasets, which Table. 4 represents their results. As shown by the results, Puzzle-AE seems to be significantly more desirable with respect to the aforementioned abilities discussed in Section 1. We also compare our method with a self-supervised learning method that has been proposed recently in Table. 5. It is obvious that our method is more practical without any need of extra expert knowledge to design extra large (72) unambiguous geometric transformations that Fig. 10 shows their brittleness.

FPR comparison for high TPR: As discussed earlier, two of the really important operating points of ROC curve are when TPR is equal to 99.0% or 99.5%. Table. 6 shows that Puzzle-AE has significantly lower FPR in those two mentioned points in comparison with LSA [30], while their difference in AUC is not as much significant.

Model stability: As it can be seen in Fig. 14, 11, 12, 13, and in different tables, the low variances mentioned in the results of the Puzzle-AE reveals the stability of our model’s performance in comparison to the other methods. It is also can be shown that because of using weight decay, the weights of our model are bounded, which consequence in being Lipschitz. Furthermore, Puzzle-AE produces smooth output. It is shown in [55] that by being Lipschitz and smooth, The convergence of ADAM optimizer [53] is theoretically provable. This means that we could achieve a highly reliable and stable model at the end of the training phase. This is not the case for other methods such as GT [23] and DSVDD [5] as shown in Table. 7, where there are large fluctuations of AUC in different epochs of the training process. Because of using unprincipled early stopping methods

TABLE 5: Comparing Puzzle AE with GT [23]. As it is shown, Puzzle AE has significantly better generalization on wide gamut of datasets.

	MNIST [41]	CIFAR-10 [16]	MVTec [24]	Head CT (hemorrhage)	Brain MRI Images (Tumor)
GT [23]	98.00	82.30	67.20	44.70*	82.07*
OURS	98.00	72.47	77.63	86.43	96.34

TABLE 6: Comparison of FPR at TPR equal to 99.5% and 0.99% between Puzzle AE and LSA [30] on the MNIST [41] dataset. As it is shown, Puzzle AE has significantly better FPR showing better applicability.

TPR	Method	0	1	2	3	4	5	6	7	8	9	Mean
99%	LSA* [30]	0.0765	0.0088	0.7238	0.4119	0.6365	0.3274	0.1190	0.4591	0.5975	0.2428	0.3603
	OURS	0.0480	0.0053	0.3295	0.2079	0.3157	0.1939	0.1086	0.2451	0.7156	0.1724	0.2342
99.5%	LSA* [30]	0.0980	0.0123	0.8178	0.4871	0.7210	0.3924	0.1587	0.5447	0.7146	0.3142	0.4261
	OURS	0.0694	0.0088	0.4079	0.2545	0.4287	0.3262	0.1441	0.2977	0.7895	0.2061	0.2932

that usually don't generalize well on unseen datasets, GT [23] AUC fluctuates near 6% on medical dataset and near 30% on MVTEC [24] dataset while its train accuracy is above 98%.

Effect of training sample size on performance: Data efficiency, as another important feature that is desired in real-world applications, is shown in Figure. 9 and Table. 8. Traditional AE based approaches usually need a rich dataset to model every complexity in data and obtain good generalization. However, As Fig. 9 illustrates, Puzzle-AE is significantly better than LSA [30] and DAE [56] in terms of data efficiency that is because of its different mean to model abstractions. It is also shown in Table. 8 that not only Puzzle-AE is significantly better than other SOTA AE based approaches but also, is better than DSVDD [5] that is a one-class method.

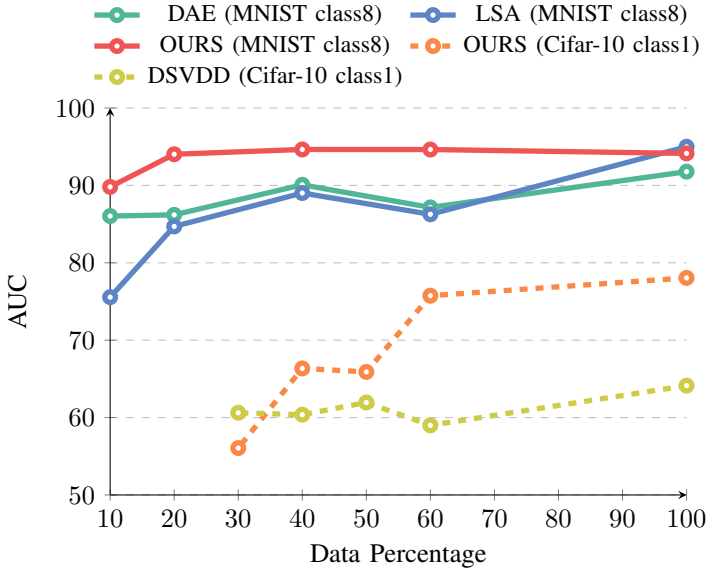


Figure 9: Data efficiency plots. As it is shown, Puzzle AE is significantly more data efficient than LSA [30] and DAE [56] on the class 8 of the MNIST [41] dataset. Puzzle AE also performs better than DSVDD [5] in the class car of the CIFAR-10 [16] dataset.

Robustness through attacked normal samples: Robustness against attacked normal images is examined and the results are reported in Fig. 10. As it is shown, Puzzle-AE is significantly more robust against attacks to normal images with three different values of ϵ (0.05, 0.1 and 0.2) in comparison to LSA [30],

ARAE [15] and GT [23]. To explain different attack applied to our method in attack1, we apply FGSM [38] attack on the normal class before permutation. However, in attack2, we apply FGSM [38] attack on the permuted image then attacked image is brought back to the original form by using corresponding inverse permutation. By getting average over all possible permutations, the attacked version of the normal class is obtained.

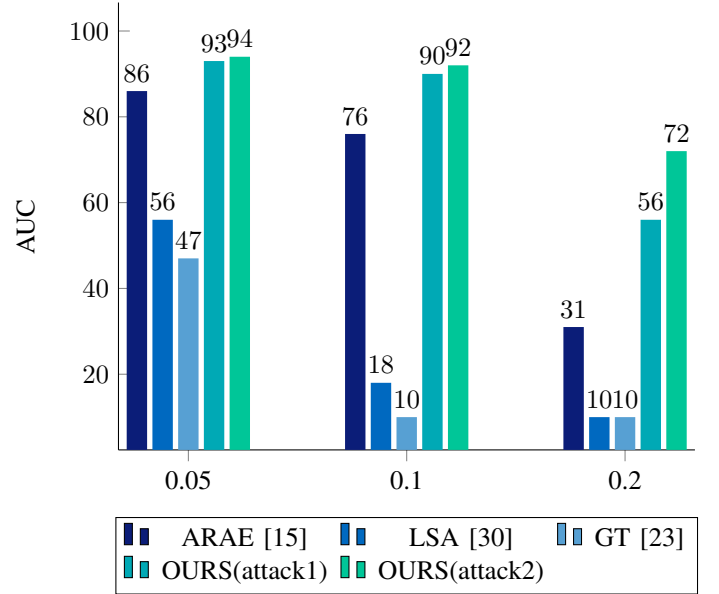


Figure 10: Robustness to adversarial attack on normal data at testing time. The results are shown for three different ϵ and the model is trained on the class 8 of the MNIST [41] dataset. Clearly, Puzzle AE is significantly more robust than other SOTAs on the most challenging class of the MNIST [41] dataset.

Effect of each component of the proposed method on final performance: Finally, Table. 9 shows the effect of every single module or algorithm that has been used in this framework on CIFAR-10 [16] dataset. The results are shown for puzzle-solving AE (PAE), puzzle-solving and colorization (CPAE), and also CPAE combined with adversarial training (CPAE-G). As it can be seen, each of these parts has an important role and makes a significant contribution for gaining the best possible performance.

TABLE 7: Up - GT [23] AUC fluctuations during training procedure on head ct medical and the capsule class of MVTecAD [24] dataset. Bottom - DSVDD [5] AUC fluctuations during last 16 epochs of training procedure on the class car of CIFAR-10 [16] dataset.

Method	Dataset		0	1	2	3	4	5	6	7	8	9	10	11	12	13	14	15	16
GT [23]	Head CT	AUC	56.52	53.68	54.26	69.29	67.10	69.87	77.48	79.03	76.45	77.48	79.55	80.06	81.23	80.90	77.68	79.23	75.03
		Train ACC	14.59	34.45	43.41	55.84	71.17	90.08	98.88	99.92	99.98	100	100	100	100	100	99.93	99.60	98.14
	MVTec (Capsule)	AUC	45.95	67.41	71.20	74.11	77.46	60.75	64.10	73.00	73.00	62.82	62.50	66.29	69.49	60.63	66.85	73.35	68.93
		Train ACC	98.89	99.50	100	100	100	99.99	100	100	100	100	100	99.55	100	98.49	100	100	100
DSVDD [5]	Cifar-10 (Car)	AUC	56.21	51.83	53.74	54.50	57.57	59.86	60.23	60.60	59.81	56.37	57.72	55.82	58.40	54.04	54.97	55.25	56.22
		Train loss	0.577	0.477	0.387	0.332	0.328	0.314	0.306	0.300	0.288	0.282	0.267	0.259	0.251	0.242	0.229	0.218	0.211

TABLE 8: Comparing Puzzle AE with LSA [30] and DSVDD [5]. Both are trained on the MNIST [41] dataset with only 1/12 of the original training samples.

Method	0	1	2	3	4	5	6	7	8	9	mean
LSA* [30]	95.93 \pm 0.087	99.82 \pm 0.005	80.95 \pm 0.119	83.95 \pm 0.090	87.59 \pm 0.113	85.81 \pm 0.072	92.61 \pm 0.059	93.31 \pm 0.074	76.56 \pm 0.328	92.40 \pm 0.075	88.89
DSVDD* [5]	96.10 \pm 0.057	99.17 \pm 0.006	88.62 \pm 0.146	86.60 \pm 0.252	95.09 \pm 0.024	84.93 \pm 0.091	96.40 \pm 0.058	94.68 \pm 0.036	89.76 \pm 0.121	94.72 \pm 0.044	92.61
OURS	99.54 \pm 0.044	99.73 \pm 0.034	90.41 \pm 0.593	89.59 \pm 1.056	95.71 \pm 0.306	96.79 \pm 0.504	97.23 \pm 0.310	96.98 \pm 0.189	89.81 \pm 0.676	93.17 \pm 0.592	94.90

TABLE 9: Effect of each component or algorithm is illustrated separately. As it is shown, CPAE-G has the best results on sample dataset CIFAR-10 [16].

		0	1	2	3	4	5	6	7	8	9	mean
MIN	puzzle AE (PAE)	76.32	69.69	68.70	54.08	75.30	62.91	72.72	69.61	80.87	64.88	69.51
	colorization + puzzle (CPAE)	79.51	69.77	68.51	54.75	72.56	63.24	67.86	68.30	82.09	65.57	69.22
	colorization + puzzle + GAN (CPAE-G)	79.42	73.00	69.48	53.00	73.98	65.13	68.98	70.65	83.28	66.73	70.37
MAX	puzzle AE (PAE)	76.29	69.07	68.19	52.14	75.84	60.84	73.66	68.61	78.26	66.20	68.91
	colorization + puzzle (CPAE)	78.87	76.56	67.97	54.33	74.69	62.32	75.72	71.59	81.06	70.92	71.40
	colorization + puzzle + GAN (CPAE-G)	77.21	77.31	69.3	54.10	74.76	64.10	76.02	70.42	81.04	66.91	71.12
AVG	puzzle AE (PAE)	76.59	68.84	68.54	53.00	76.00	61.8	73.32	68.87	79.54	66.12	69.26
	colorization + puzzle (CPAE)	79.72	75.86	68.56	54.74	74.87	64.21	74.02	72.97	82.64	70.62	71.82
	colorization + puzzle + GAN (CPAE-G)	78.93	78.05	69.95	54.88	75.46	66.04	74.76	73.30	83.34	69.96	72.47

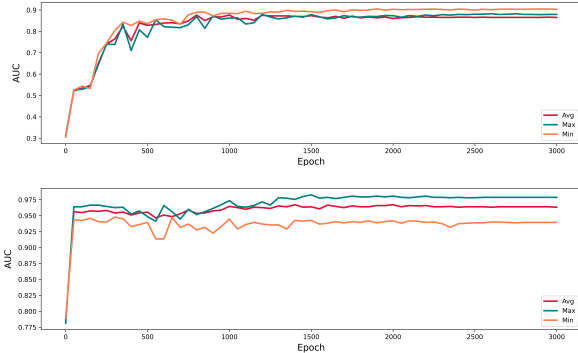


Figure 11: Min, max and avg AUC Plots with respect to training epochs are shown for each medical dataset. As it is obvious, training procedure continues till the convergence of all of the AUC plots.

5. Ablation

Effect of several important parameters has been examined in this study. Each of which is as follows:

- 1) **Effect of simple architectural changes on performance:** It is observed that by halving the number of filters in each layer, performance doesn't drop significantly specifically for MNIST [41], Fashion-MNIST [43] and COIL-100 [46] datasets. Hence, if testing time or testing memory is important for a simple real world

application, it can be halved without any significant performance drop.

- 2) **Effect of training sample size on performance:** It is observed that by dividing number of training samples to 12 in MNIST [41] dataset, performance drop is only near 3.1 percentage. Fig. 9 and Table. 8 show the results of the puzzle AE on MNIST [41] and the class car of the CIFAR-10 [16] dataset.
- 3) **Effect of converting pictures to gray-scale on performance:** It is observed that extracted normal features of Puzzle-AE are less sensitive to color for some specific classes of the CIFAR-10 [16] dataset. For example, there is no significant performance drop observed on the class car of the CIFAR-10 [16] when converting the whole dataset to black and white. Fig. 8 shows the interesting ability of the proposed model in solving unseen black and white puzzled inputs.
- 4) **Effect of changing activation functions on performance:** In contrast to some of the SOTA frameworks, it is observed that there is no significant performance drop when changing activation functions of our base model (standard U-Net [35]) to elu [57] in Puzzle-AE.
- 5) **Effect of PGD [25], FGSM [38] and random noise on performance:** It is observed that PGD [25] and FGSM [38] have almost similar effects on the performance. However, random noise can't remove shortcuts completely leading to overfitting on some classes of the CIFAR-10 [16] like the car class.

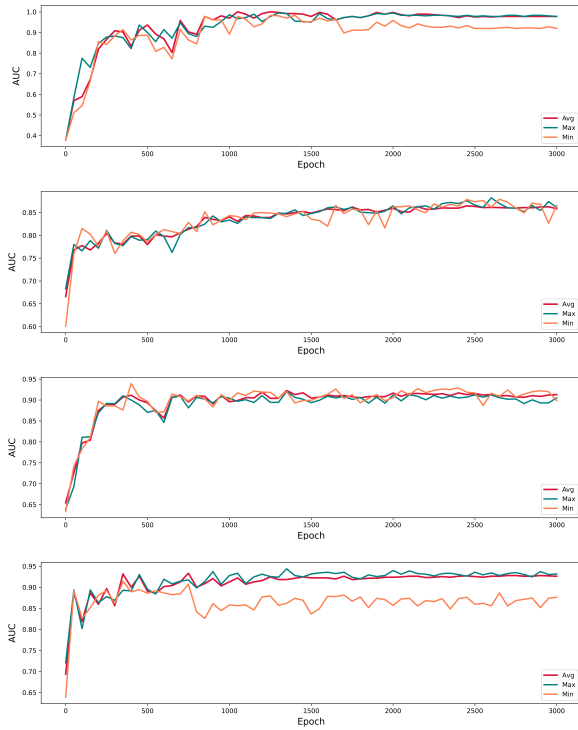


Figure 12: Min, max and avg AUC Plots with respect to training epochs are shown for the classes toothbrush, transistor, hazelnut and bottle of the MVTecAD [24] dataset. As it is obvious, training procedure continues till the convergence of all of the AUC plots.

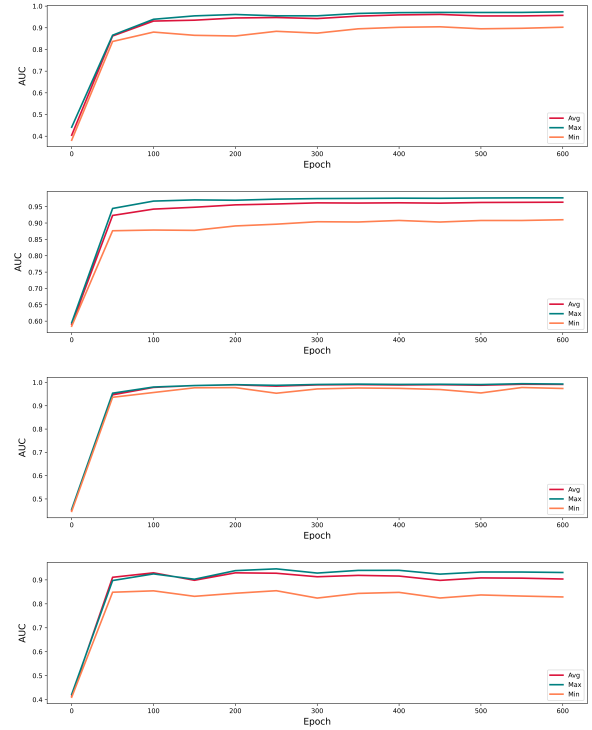


Figure 13: Min, max and avg AUC Plots with respect to training epochs are shown for the classes 2, 4, 6 and 8 of the MNIST [41] dataset.

6. Conclusion and Future Work

In this study a simple yet very effective framework is introduced. It is strived to reduce generalization ability on anomalous samples while increasing generalization on normal ones by using adversarial robust training and self-supervised learning. Results show significant improvement on stability, robustness, data efficiency, generality and FPR at high TPRs on wide gamut of datasets from medical imaging to MVTecAD [24] and CIFAR-10 [16]. However, there are still some deficiencies that solving them could improve the current results significantly. For example, shortcut problem hasn't been solved completely yet and there are still some anomalous samples that their puzzles are solved by the model perfectly. There is also a lack of quantitative criterion for deciding between choosing min, max or average, which could be confusing specially in medical applications with extra low number of training datum. Left group of Fig. 7 and Fig. 11 show the mentioned problems that need to be solved in future works.

Acknowledgments

The authors would like to thank Soroosh Baselizadeh and Amirreza Shaeiri for their insightful comments and reviews of this work.

References

- [1] R. Chalapathy and S. Chawla, "Deep learning for anomaly detection: A survey," *arXiv preprint arXiv:1901.03407*, 2019.
- [2] X. Chen and E. Konukoglu, "Unsupervised detection of lesions in brain mri using constrained adversarial auto-encoders," *arXiv preprint arXiv:1806.04972*, 2018.

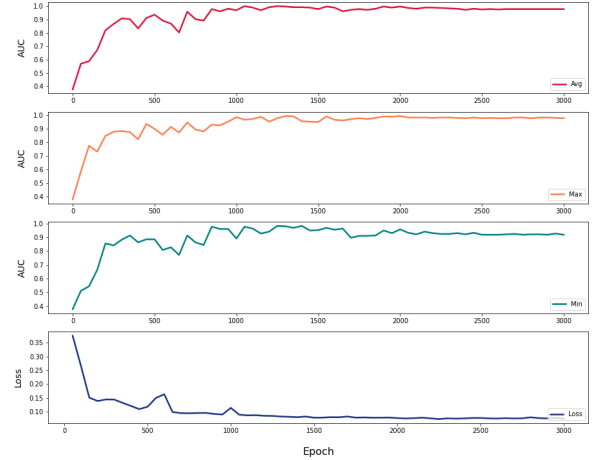


Figure 14: Min, max and avg AUC Plots with respect to training epochs are shown for the toothbrush class of the MVTecAD [24] dataset. As it is obvious, training procedure continues till the convergence of all of the AUC plots and also loss value.

- [3] C. Baur, B. Wiestler, S. Albarqouni, and N. Navab, "Deep autoencoding models for unsupervised anomaly segmentation in brain mr images," in *International MICCAI Brainlesion Workshop*. Springer, 2018, pp. 161–169.
- [4] D. Gong, L. Liu, V. Le, B. Saha, M. R. Mansour, S. Venkatesh, and A. v. d. Hengel, "Memorizing normality to detect anomaly: Memory-augmented deep autoencoder for unsupervised anomaly detection," in *Proceedings of the IEEE International Conference on Computer Vision*, 2019, pp. 1705–1714.
- [5] L. Ruff, R. Vandermeulen, N. Goernitz, L. Deecke, S. A. Siddiqui,

- A. Binder, E. Müller, and M. Kloft, “Deep one-class classification,” in *International conference on machine learning*, 2018, pp. 4393–4402.
- [6] Y. Chen, X. S. Zhou, and T. S. Huang, “One-class svm for learning in image retrieval,” in *Proceedings 2001 International Conference on Image Processing (Cat. No. 01CH37205)*, vol. 1. IEEE, 2001, pp. 34–37.
- [7] M. Sabokrou, M. Khalooei, M. Fathy, and E. Adeli, “Adversarially learned one-class classifier for novelty detection,” in *Proceedings of the IEEE Conference on Computer Vision and Pattern Recognition*, 2018, pp. 3379–3388.
- [8] I. J. Goodfellow, J. Shlens, and C. Szegedy, “Explaining and harnessing adversarial examples,” *arXiv preprint arXiv:1412.6572*, 2014.
- [9] I. Goodfellow, “Nips 2016 tutorial: Generative adversarial networks,” *arXiv preprint arXiv:1701.00160*, 2016.
- [10] N. Kodali, J. Abernethy, J. Hays, and Z. Kira, “On convergence and stability of gans,” *arXiv preprint arXiv:1705.07215*, 2017.
- [11] T. Salimans, I. Goodfellow, W. Zaremba, V. Cheung, A. Radford, and X. Chen, “Improved techniques for training gans,” in *Advances in neural information processing systems*, 2016, pp. 2234–2242.
- [12] A. Martin and B. Lon, “Towards principled methods for training generative adversarial networks,” in *NIPS 2016 Workshop on Adversarial Training. In review for ICLR*, vol. 2016, 2017.
- [13] E. Nalisnick, A. Matsukawa, Y. W. Teh, D. Gorur, and B. Lakshminarayanan, “Do deep generative models know what they don’t know?” *arXiv preprint arXiv:1810.09136*, 2018.
- [14] M. Sakurada and T. Yairi, “Anomaly detection using autoencoders with nonlinear dimensionality reduction,” in *Proceedings of the MLSDA 2014 2nd Workshop on Machine Learning for Sensory Data Analysis*, 2014, pp. 4–11.
- [15] M. Salehi, A. Arya, B. Pajoum, M. Otoofi, A. Shaeiri, M. H. Rohban, and H. R. Rabiee, “Arae: Adversarially robust training of autoencoders improves novelty detection,” *arXiv preprint arXiv:2003.05669*, 2020.
- [16] A. Krizhevsky, V. Nair, and G. Hinton, “Cifar-10 (canadian institute for advanced research),” 2009.
- [17] R. Hamaguchi, K. Sakurada, and R. Nakamura, “Rare event detection using disentangled representation learning,” in *Proceedings of the IEEE Conference on Computer Vision and Pattern Recognition*, 2019, pp. 9327–9335.
- [18] J. Deng, W. Dong, R. Socher, L.-J. Li, K. Li, and L. Fei-Fei, “Imagenet: A large-scale hierarchical image database,” in *2009 IEEE conference on computer vision and pattern recognition*. Ieee, 2009, pp. 248–255.
- [19] Z. Wu, Y. Xiong, S. X. Yu, and D. Lin, “Unsupervised feature learning via non-parametric instance discrimination,” in *Proceedings of the IEEE Conference on Computer Vision and Pattern Recognition*, 2018, pp. 3733–3742.
- [20] A. v. d. Oord, Y. Li, and O. Vinyals, “Representation learning with contrastive predictive coding,” *arXiv preprint arXiv:1807.03748*, 2018.
- [21] R. Zhang, P. Isola, and A. A. Efros, “Split-brain autoencoders: Unsupervised learning by cross-channel prediction,” in *Proceedings of the IEEE Conference on Computer Vision and Pattern Recognition*, 2017, pp. 1058–1067.
- [22] S. A. Taghanaki, M. Havaei, A. Lamb, A. Sanghi, A. Danielyan, and T. Custis, “Jigsaw-vae: Towards balancing features in variational autoencoders,” *arXiv preprint arXiv:2005.05496*, 2020.
- [23] I. Golan and R. El-Yaniv, “Deep anomaly detection using geometric transformations,” in *Advances in Neural Information Processing Systems*, 2018, pp. 9758–9769.
- [24] P. Bergmann, M. Fauser, D. Sattlegger, and C. Steger, “Mvtec ad—a comprehensive real-world dataset for unsupervised anomaly detection,” in *Proceedings of the IEEE Conference on Computer Vision and Pattern Recognition*, 2019, pp. 9592–9600.
- [25] A. Madry, A. Makelov, L. Schmidt, D. Tsipras, and A. Vladu, “Towards deep learning models resistant to adversarial attacks,” *arXiv preprint arXiv:1706.06083*, 2017.
- [26] A. Ilyas, S. Santurkar, D. Tsipras, L. Engstrom, B. Tran, and A. Madry, “Adversarial examples are not bugs, they are features,” in *Advances in Neural Information Processing Systems*, 2019, pp. 125–136.
- [27] M. Noroozi and P. Favaro, “Unsupervised learning of visual representations by solving jigsaw puzzles,” in *European Conference on Computer Vision*. Springer, 2016, pp. 69–84.
- [28] D. Hendrycks, M. Mazeika, S. Kadavath, and D. Song, “Using self-supervised learning can improve model robustness and uncertainty,” in *Advances in Neural Information Processing Systems*, 2019, pp. 15 663–15 674.
- [29] O. Ronneberger, P. Fischer, and T. Brox, “U-net: Convolutional networks for biomedical image segmentation,” in *International Conference on Medical image computing and computer-assisted intervention*. Springer, 2015, pp. 234–241.
- [30] D. Abati, A. Porrello, S. Calderara, and R. Cucchiara, “Latent space autoregression for novelty detection,” in *Proceedings of the IEEE Conference on Computer Vision and Pattern Recognition*, 2019, pp. 481–490.
- [31] P. Perera, R. Nallapati, and B. Xiang, “Ocgan: One-class novelty detection using gans with constrained latent representations,” in *Proceedings of the IEEE Conference on Computer Vision and Pattern Recognition*, 2019, pp. 2898–2906.
- [32] T. Schlegl, P. Seeböck, S. M. Waldstein, U. Schmidt-Erfurth, and G. Langs, “Unsupervised anomaly detection with generative adversarial networks to guide marker discovery,” in *International conference on information processing in medical imaging*. Springer, 2017, pp. 146–157.
- [33] S. Akcay, A. Atapour-Abarghouei, and T. P. Breckon, “Ganomaly: Semi-supervised anomaly detection via adversarial training,” in *Asian Conference on Computer Vision*. Springer, 2018, pp. 622–637.
- [34] D. P. Kingma and M. Welling, “Auto-encoding variational bayes,” *arXiv preprint arXiv:1312.6114*, 2013.
- [35] X. Li, H. Chen, X. Qi, Q. Dou, C.-W. Fu, and P.-A. Heng, “H-denseunet: hybrid densely connected unet for liver and tumor segmentation from ct volumes,” *IEEE transactions on medical imaging*, vol. 37, no. 12, pp. 2663–2674, 2018.
- [36] G. Litjens, T. Kooi, B. E. Bejnordi, A. A. A. Setio, F. Ciompi, M. Ghafoorian, J. A. Van Der Laak, B. Van Ginneken, and C. I. Sánchez, “A survey on deep learning in medical image analysis,” *Medical image analysis*, vol. 42, pp. 60–88, 2017.
- [37] X. Wang, Y. Peng, L. Lu, Z. Lu, M. Bagheri, and R. M. Summers, “Chestx-ray8: Hospital-scale chest x-ray database and benchmarks on weakly-supervised classification and localization of common thorax diseases,” in *Proceedings of the IEEE conference on computer vision and pattern recognition*, 2017, pp. 2097–2106.
- [38] E. Wong, L. Rice, and J. Z. Kolter, “Fast is better than free: Revisiting adversarial training,” *arXiv preprint arXiv:2001.03994*, 2020.
- [39] M. Sabokrou, M. Pourreza, M. Fayyaz, R. Entezari, M. Fathy, J. Gall, and E. Adeli, “Avid: Adversarial visual irregularity detection,” in *Asian Conference on Computer Vision*. Springer, 2018, pp. 488–505.
- [40] I. Tolstikhin, O. Bousquet, S. Gelly, and B. Schoelkopf, “Wasserstein auto-encoders,” *arXiv preprint arXiv:1711.01558*, 2017.
- [41] Y. LeCun, C. Cortes, and C. Burges, “Mnist handwritten digit database,” 2010.
- [42] X. Li, I. Kiringa, T. Yeap, X. Zhu, and Y. Li, “Exploring deep anomaly detection methods based on capsule net,” in *ICML 2019 Workshop on Uncertainty and Robustness in Deep Learning, At Long Beach*, 2019.
- [43] H. Xiao, K. Rasul, and R. Vollgraf, “Fashion-mnist: a novel image dataset for benchmarking machine learning algorithms,” *arXiv preprint arXiv:1708.07747*, 2017.
- [44] B. Zong, Q. Song, M. R. Min, W. Cheng, C. Lumezanu, D. Cho, and H. Chen, “Deep autoencoding gaussian mixture model for unsupervised anomaly detection,” 2018.
- [45] S. Zhai, Y. Cheng, W. Lu, and Z. Zhang, “Deep structured energy based models for anomaly detection,” *arXiv preprint arXiv:1605.07717*, 2016.
- [46] S. A. Nene, S. K. Nayar, and H. Murase, “object image library (coil-100,” *Tech. Rep.*, 1996.
- [47] P. Bergmann, S. Löwe, M. Fauser, D. Sattlegger, and C. Steger, “Improving unsupervised defect segmentation by applying structural similarity to autoencoders,” in *International Joint Conference on Computer Vision, Imaging and Computer Graphics Theory and Applications (VISIGRAPP)*, 2019.
- [48] H. Xu, C. Caramanis, and S. Sanghavi, “Robust pca via outlier pursuit,” in *Advances in Neural Information Processing Systems*, 2010, pp. 2496–2504.
- [49] M. C. Tsakiris and R. Vidal, “Dual principal component pursuit,” *The Journal of Machine Learning Research*, vol. 19, no. 1, pp. 684–732, 2018.

- [50] S. Pidhorskyi, R. Almohsen, and G. Doretto, “Generative probabilistic novelty detection with adversarial autoencoders,” in *Advances in neural information processing systems*, 2018, pp. 6822–6833.
- [51] S. Ioffe and C. Szegedy, “Batch normalization: Accelerating deep network training by reducing internal covariate shift,” *arXiv preprint arXiv:1502.03167*, 2015.
- [52] A. Radford, L. Metz, and S. Chintala, “Unsupervised representation learning with deep convolutional generative adversarial networks,” *arXiv preprint arXiv:1511.06434*, 2015.
- [53] D. P. Kingma and J. Ba, “Adam: A method for stochastic optimization,” *arXiv preprint arXiv:1412.6980*, 2014.
- [54] P. Goyal, P. Dollár, R. Girshick, P. Noordhuis, L. Wesolowski, A. Kyrola, A. Tulloch, Y. Jia, and K. He, “Accurate, large minibatch sgd: Training imagenet in 1 hour,” *arXiv preprint arXiv:1706.02677*, 2017.
- [55] X. Chen, S. Liu, R. Sun, and M. Hong, “On the convergence of a class of adam-type algorithms for non-convex optimization,” *arXiv preprint arXiv:1808.02941*, 2018.
- [56] P. Vincent, H. Larochelle, Y. Bengio, and P.-A. Manzagol, “Extracting and composing robust features with denoising autoencoders,” in *Proceedings of the 25th international conference on Machine learning*, 2008, pp. 1096–1103.
- [57] D.-A. Clevert, T. Unterthiner, and S. Hochreiter, “Fast and accurate deep network learning by exponential linear units (elus),” *arXiv preprint arXiv:1511.07289*, 2015.